Different bonding type along each crystallographic axis: Computational study of poly(*p*-phenylene terephthalamide)

Jie Yu,[1,*] Giacomo Fiorin,[2] Haowei Peng,[1] Michael L. Klein,[1,2] and John P. Perdew[1,2,†]
[1]*Department of Physics, Temple University, Philadelphia, Pennsylvania 19122, USA*
[2]*Department of Chemistry, Temple University, Philadelphia, Pennsylvania 19122, USA*

(Received 4 March 2019; revised manuscript received 25 February 2020; accepted 19 March 2020; published 4 May 2020)

Poly(*p*-phenylene terephthalamide) (PPTA) exhibits van der Waals (vdW) bonding along its *a* axis, hydrogen bonding along its *b* axis, and covalent bonding along its *c* axis. We explore the structural and mechanical properties of PPTA using density functional theory with various functionals including LDA, PBE, PBE+rVV10L, SCAN, and SCAN+rVV10, compared with available experiments. The hierarchy of nonempirical semilocal functionals LDA, PBE, and SCAN (not fitted to any multicenter bonded system) includes differing amounts of intermediate-range vdW interaction. rVV10 is the long-range vdW correction. (rVV10L differs from rVV10 only in the value of a range parameter.) Among the tested functionals, SCAN shows the best performance for the lattice parameters of PPTA along the two crystal directions involving vdW or hydrogen-bond interaction. The equilibrium lattice constants obtained by SCAN and PBE+rVV10L are closest to experimental data, while SCAN+rVV10 slightly overbinds the system. We study the mechanical response of PPTA by applying strain along three lattice directions. Due to the inclusion of vdW interaction, SCAN, PBE+rVV10L, and SCAN+rVV10 all exhibit correct bonding strain-energy curves. On the contrary, PBE strongly underestimates the vdW interaction needed to resist uniaxial stretching along the *a* axis. The Young's modulus and yield strength of PPTA are computed and compared with previous results. The experimental values are much smaller than the computed ones, mainly due to the fact that the PPTA fiber samples used for measurements are mechanically weaker than the perfect molecular crystals considered in the simulations. Interestingly, when a compressive uniaxial stress of 25 Kbar is applied along the *b* axis, a structural phase transition, in which the hydrogen bonds reform along one diagonal of the *ab* rectangle, is predicted by SCAN.

DOI: 10.1103/PhysRevMaterials.4.055601

I. INTRODUCTION

Poly(*p*-phenylene terephthalamide) (PPTA) fiber [1,2], commercially known as Kevlar®, exhibits high mechanical strength and large modulus arising from a highly anisotropic crystal structure consisting of covalent bonds, hydrogen bonds, and van der Waals (vdW) interactions along its *c*, *b*, and *a* axes, respectively. As a result, it finds uses as a protective material, e.g., in helmets. Since its discovery in the early 1950s, PPTA fibers have drawn much attention due to their excellent mechanical properties [3–6]. Experimentally, various techniques including x-ray diffraction (XRD) [5,7,8], electron diffraction, and electron microscope [9] techniques have been utilized to explore the structure of PPTA fibers. Lattice constants of PPTA crystal have been measured experimentally using XRD technique [8]. The radial structure of PPTA fibers was explored using interference microscopy [10] and the orientation of PPTA chains was characterized using fluorescence depolarization technique [11]. The relationship between the microstructure of PPTA fibers and their excellent tensile strength has been investigated with Raman spectroscopy [4,12], x-ray diffraction [13], and atomic force microscopy [14] techniques.

The mechanical properties of PPTA are highly correlated with the unique bonding structure in the PPTA crystal. The orthorhombic PPTA crystal structure was proposed containing two-molecule repeating units that form chains through strong chemical bonds along the *c* direction [5,7,8]. Due to the close proximity of the chains, hydrogen bonds are formed between the neighboring NH and CO groups along the *b* axis, forming sheets. Along the *a* or intersheet axis, the interchain interaction is dominated by the vdW force. Therefore, from a mechanical point of view, the crystal is anisotropic and is stronger along the chain direction while much weaker in the other two directions of the unit cell. Computationally, it is thus desirable to apply a computational method that can treat these three types of interactions equally well.

Theoretical computation is an essential tool for structural studies of PPTA [15–17]. For instance, structural properties of a set of 16 PPTA structures with systematic variation of four structural motifs with the same crystal lattice have been carried out using PBE and the nonlocal vdW-DF2 with the rPW86 exchange functional [15]. First-principles calculations using the B3LYP-D and PBE0-D functionals, where D indicates an empirical correction for dispersion interactions, have been performed to study the structural and mechanical

*jieyu@temple.edu
†perdew@temple.edu

properties of PPTA [17], predicting a theoretical Young's modulus of 252 GPa for the PPTA crystal.

Theoretical description of molecular crystals relies on the accurate treatment of noncovalent interactions [18]. The intermolecular interactions in these crystals are dominated by the hydrogen bonding and van der Waals (vdW) interactions. Standard approximations within density functional theory (DFT) tend to give unsatisfactory performance in the description of weak interactions, greatly limiting their applications for the study of molecular crystals [19].

Recently, a new functional called SCAN (strongly constrained and appropriately normed) metageneralized gradient approximation (meta-GGA) has been developed [20]. SCAN is designed to satisfy 17 exact constraints, and is not fitted to any multicenter bonded system. The goal of SCAN is to predict bonds, not to fit them. While nonempirical functionals are not always more accurate than empirical ones, they can be more predictive over a wide range of systems and properties. With the capability to accurately describe covalent, metallic, and weak bonds near equilibrium [21], the SCAN functional can serve as a powerful nonempirical tool for predicting the structures of molecular crystals. We will demonstrate this here for PPTA, and then apply SCAN to predict a structural phase transition in PPTA under a uniaxial compressive stress along the hydrogen-bond or *b* axis.

Computationally efficient semilocal functionals like the local density approximation (LDA) [22], the Perdew-Burke-Ernzerhof (PBE) GGA [23], and SCAN cannot capture the long-range part of the vdW attraction, but SCAN can estimate the interactions between atoms at typical vdW equilibrium bond lengths (around 3 Å). As discussed in Ref. [23], SCAN achieves this through the exchange part of the exchange-correlation energy. While this is disturbing from a correlated wave function viewpoint (and not without problems [24]), it is natural from the viewpoint of semilocal density functionals. Both exact exchange alone and exact correlation alone are fully nonlocal functionals, but the nonlocality in isolated atoms is limited by the requirement that the exact exchange and correlation holes lie inside the atomic densities, so SCAN is very accurate for exchange alone and correlation alone in such atoms. In multicenter systems like molecules or solids, the nonlocalities of exact exchange alone and exact correlation alone (i.e., longer-ranged features of the exact exchange and correlation holes) manifest more strongly, but tend to cancel on the length scale of equilibrium bond lengths. This well-understood cancellation makes SCAN accurate for the exchange-correlation energies of covalent or noncovalent bonds near equilibrium, although it is not accurate for exchange or correlation separately. For instance, SCAN is better than PBE or PBE with a long-range vdW correction for the change in hydrogen-bond network that occurs in liquid water at an interface with solid Al_2O_3 [25].

A popular alternative to SCAN is to start from a dispersionless semilocal functional, and then add to it a fully nonlocal correction to account for nearly all of the van der Waals interaction. This is necessarily an empirical approach, fitted to van der Waals–bonded systems. Our goal with SCAN is to describe bonds without fitting to any bonded systems.

The long-range vdW correction to SCAN is relatively unimportant near equilibrium, but it becomes more important in the stretched-bond and dissociation limits. For this reason, we do not stress the long-range correction here, apart from a demonstration that it is important near equilibrium only for PBE and not for SCAN. To do this, we employ the rVV10 [26,27] long-range correction, not because we claim it is optimal but because its short-range cutoff parameter has been fitted separately for PBE [23] and for SCAN [28]. There has been much progress on long-range corrections (e.g., Refs. [29–50]), some of which is summarized in Sec. A of the Supplemental Material [51]. But it is still not clear which if any of the proposed corrections is both correct at long-range and compatible with SCAN at intermediate range. That is a subject for future investigation and perhaps future functional development.

The addition of long-range vdW interaction, in the revised form of the Vydrov–Van Voorhis nonlocal correlation functional (rVV10) [26], to the Perdew, Burke, and Ernzerhof GGA (PBE) [52] and to SCAN (PBE+rVV10L and SCAN+rVV10, respectively) [23,28], is also considered here. PBE+rVV10L was originally optimized for layered materials, but produces a very small mean absolute percentage error (about 2%) for the interaction energies of the seven hydrogen-bonding molecular dimers in the S22 data set [23]. In this work, we systematically study the structural and mechanical properties of PPTA using a comprehensive set of functionals, including the local density approximation (LDA) [22], PBE, PBE+rVV10L [23], SCAN [20], and SCAN+rVV10 [28].

The mechanical response of the PPTA molecular crystal under uniaxial strain or uniaxial stress along three crystal directions is explored to provide a clear picture of the bonding nature in PPTA as well as the interplay between three different types of interactions and the mechanical responses of the crystal. We further predict a phase transition due to compressive strain that leads to a change of axis for the hydrogen-bond network within the PPTA crystal.

II. COMPUTATIONAL DETAILS

The first-principles calculations are based on density functional theory (DFT) using the Vienna software package (VASP) [53] with the plane-wave projector augmented-wave (PAW) pseudopotentials [54]. We adopt a $6 \times 6 \times 6$ Monkhorst-Pack *k*-point mesh for the integrations over the Brillouin zone and an energy cutoff of 520 eV is used in all calculations. For the structural relaxation calculations, the forces on each atom are less than 0.01 eV $Å^{-1}$. In the study of the strain-energy relation, we apply uniaxial strain by increasing or decreasing the lattice constant along a given direction while keeping those for other directions unchanged. When applying uniaxial stress to the system, we change the lattice constant along a given direction while the lattice constants along the other two directions are fully optimized.

III. RESULTS AND DISCUSSIONS

PPTA has a periodic crystal structure with a monoclinic (pseudo-orthorhombic) unit cell [8] and the chemical formula $[\text{-CO-C}_6\text{H}_4\text{-CO-NH-C}_6\text{H}_4\text{-NH-}]_n$. PPTA contains C, N, H, and O atoms and the *ab* and *ac* planes of the cell are shown in Fig. 1. The lattice parameter of the cell along the chain

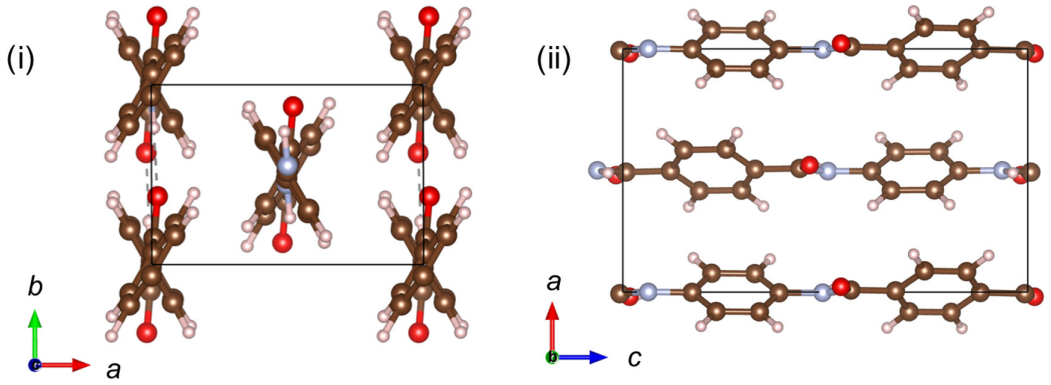

FIG. 1. View of (i) the *ab* plane and (ii) the *ac* plane of the PPTA crystal. Carbon, nitrogen, oxygen, and hydrogen atoms are rendered in brown, gray, red, and white, respectively.

direction (*c* direction) is measured to be 12.9 Å experimentally [8]. As mentioned above, those molecular chains are connected by intermolecular hydrogen bonds between the carbonyl groups and the N-H centers. The lattice parameter of the cell along this direction is 5.18 Å experimentally. These hydrogen bonds connect these chains to form sheet structures. The interaction between these sheets is dominated by vdW interactions, while the distance between the sheets is around 7.87 Å [8]. The space group number for the PPTA structure we studied is 7 (*P1c1*).

We carried out DFT calculations to relax the crystal structure of PPTA by minimizing the stress (actually the sum of the squares of the elements of the stress tensor) in the unit cell using different functionals including LDA, PBE, PBE+rVV10L, SCAN, and SCAN+rVV10, and compare our results with experimental data as shown in Table I. PPTA is an ideal model system that contains covalent bonds, hydrogen bonds, and vdW interactions along three lattice directions. Along the chain direction (*c* direction), most of the functionals perform well compared with experimental data. LDA, which strongly overestimates intermediate-range vdW attraction, thus strongly underestimates the lattice constant *a*, and will not be considered further. Along the vdW interaction direction (*a* direction), SCAN and PBE+rVV10L give better lattice constants than the other functionals. The comparison clearly shows that SCAN indeed captures a large amount of medium-range vdW interaction and can therefore accurately describe the structural properties of the PPTA crystal. SCAN+rVV10 seems to overbind the crystal, which results in a smaller value for *a*, compared with experimental data. Along the hydrogen-bond interaction direction *b*, SCAN also describes the equilibrium lattice constant very well. Overall, SCAN gives the best performance for the lattice constants of PPTA.

TABLE I. Equilibrium lattice constants of PPTA, found by stress minimization within the VASP code. Experimentally measured lattice parameters [8] are included for comparison.

	a (Å)	*b* (Å)	*c* (Å)	α (deg)
EXP[a]	7.87	5.18	12.9	90
LDA	7.30	4.96	12.91	90.0
PBE	9.71	5.14	13.05	90.7
PBE+rVV10L	7.61	5.33	13.05	90.1
SCAN	7.75	5.10	12.96	90.2
SCAN+rVV10	7.21	5.08	12.95	90.0

[a]Reference [8].

Besides the theoretical exploration of lattice parameters, we theoretically studied the mechanical response of PPTA by applying strains along three lattice directions deviating from the theoretical equilibrium lattice constants (Fig. 2). A uniaxial strain is applied along a given lattice direction, while the lattice constants in the other two directions are constrained. Along the *a* direction, the PBE functional does not capture the vdW interaction needed to give a correct bonding energy curve. SCAN, PBE+rVV10L, and SCAN+rVV10 all exhibit correct bonding energy curves. The energy minima of SCAN and PBE+rVV10L are also close to the experimental equilibrium value. It is observed that the SCAN result agrees better with experiment than SCAN +rVV10. The energy curve of SCAN+ rVV10 shows that the vdW interaction through the addition of rVV10 to SCAN slightly overbinds the system and results in a smaller lattice constant *a*.

Because the *a* lattice constant from PBE is so much bigger than the experimental one, it was necessary to perform not one but a series of stress minimizations for PBE, with the output lattice constants for one minimization as the input lattice constants for the next one, until convergence was reached.

Along the *b* or hydrogen-bond direction, as shown in Fig. 2(ii), the SCAN functional predicts the energy minimum at a lattice constant slightly smaller than the experimental value. That is consistent with the fact that SCAN slightly overestimates the strengths of hydrogen bonds due to the self-interaction error [21]. The hydrogen-bond interaction energy is slightly enhanced by SCAN+rVV10 [28], which gives an energy minimum at an even smaller lattice constant. Therefore, SCAN provides a slightly better agreement with experiment than SCAN+rVV10. The PBE+rVV10L result is slightly larger than the experimental value. The energy minimum from the PBE calculation is actually close to the experimental value. In a previous paper [54], it was pointed out that the reliability of PBE for the description of hydrogen bonds is closely connected to the bond directionality (i.e., the donor-H···acceptor angle). In our case, the N-H···O is close to a linear arrangement, which may be responsible for the acceptable performance of PBE.

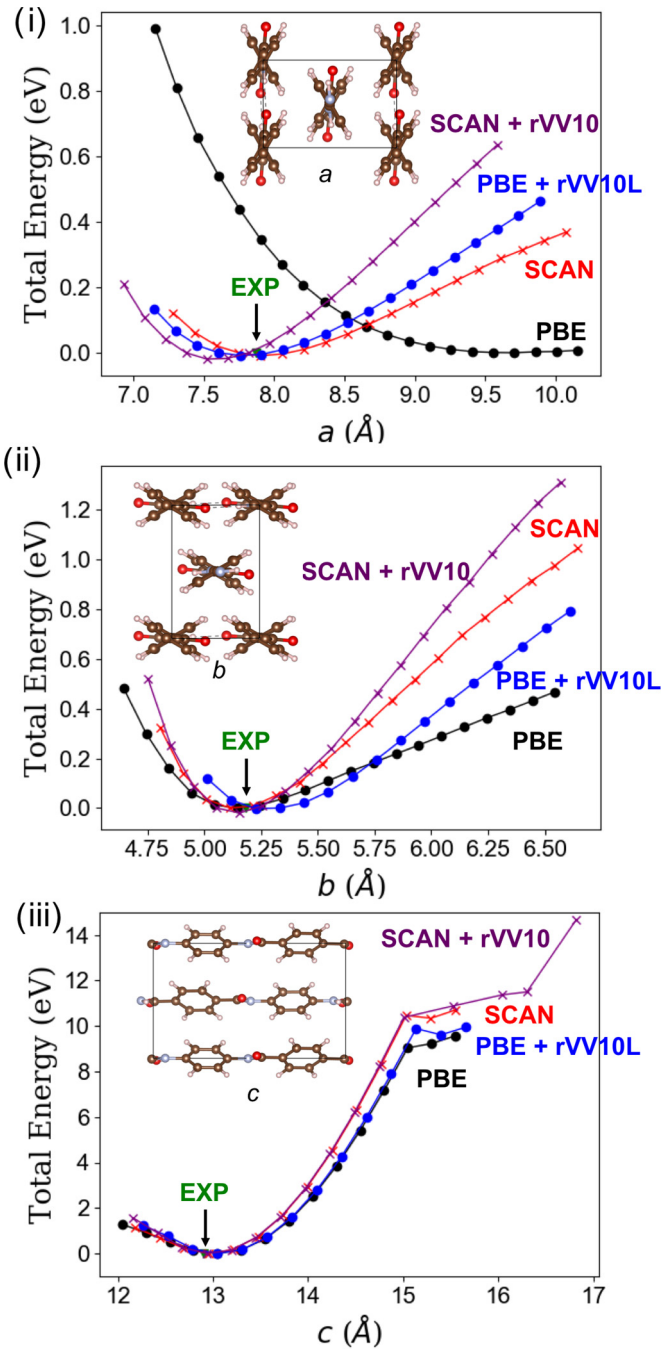

FIG. 2. Calculated strain-energy curves along the (i) a direction, (ii) b direction, and (iii) c direction using the PBE (black dot), PBE + rVV10L (blue dot), SCAN (red cross), and SCAN+rVV10 (purple cross) functionals. As one of the lattice constants is strained, the other two are held fixed for a given functional at the values shown in Table I. The experimental lattice constants are shown by the green arrows. Note that the vertical scale (energy per unit cell referred to that of unstrained cells) is very different for parts (i), (ii), and (iii). Bond breaking occurs at around $c = 15$ Å.

Along the c or molecular-chain direction, it is not surprising to observe that all four functionals behave similarly and they all give similar energy minima which are close to experimental data. The energy variation in the strain range (−6% to 30%) as shown in Fig. 2(iii) is rather large (on the scale of 10 eV), which indicates that the pulling strength along the c direction is very high and a significant amount of energy is required to stretch the material. This observation is consistent with the high pulling strength and outstanding mechanical performance of Kevlar® samples with molecular chains aligned along the c direction.

In general, SCAN predicts the lattice constants of the PPTA crystal very well compared with experiment and dramatically improves the GGA-level description provided by PBE. This indicates that SCAN can describe three different types of interactions in the crystal to a satisfactory degree quantitatively. The addition of rVV10 to SCAN results in a similar but slightly smaller unit cell and does not produce better lattice parameters compared with SCAN. We find that SCAN works better for PPTA than does SCAN+rVV10. Similar conclusions have been reached for liquid water [55,56] and also for some molecular crystals and nanostructures [57,58]. Therefore, we propose that SCAN can serve as a work horse for the quantitative study of structural and mechanical behaviors of PPTA crystals. (For bulk transition metals [59,60], however, SCAN seems to work less well than PBE, so a general-purpose revised SCAN is under construction [61].)

Why does SCAN sometimes work better than SCAN+rVV10 [62]? The short-range damping of rVV10 can be adapted to work well for a given semilocal functional in some situations, but it is only a hope that it should do so in all situations. SCAN by itself seems good enough to predict the equilibrium geometries of molecular and layered [28] materials, and the long-range rVV10 correction to SCAN has a small effect there that that may or may not be beneficial for equilibrium geometries, although it is very much needed for the exfoliation energies of layered materials [28]. For molecules and graphene physisorbed on the surfaces of metals and layered materials, the damped Zaremba-Kohn (vdW-dZK) correction [32,62–64] seems to work much better with SCAN than rVV10 does. vdW-dZK is complicated, and requires material-dependent input parameters, but captures screening effects and nonpairwise interactions better than rVV10 does.

PPTA is known to have very high pulling strength and a relatively weak compressive strength. A question would be what happens if a large-enough compressive strain is applied separately along each of the three axes of the PPTA lattice? We apply a large compressive strain ranging up to 30% and study two distinct cases which represent two extreme conditions (sudden or adiabatic) of the mechanical response. In the first case, a uniaxial strain is applied along a given lattice direction, while the other two directions are constrained, as illustrated by the black curve in Fig. 3. The other simulation condition represents a uniaxial stress applied to the system, where the lattice constants along the other two directions are fully optimized as the mechanical response to the uniaxial strain, as shown by the red curve in Fig. 3. Because the applied strain energies are released by lattice relaxation along the other two directions, total energies of systems under uniaxial stress are observed to be always lower than those of systems under uniaxial strain.

Along the chain direction c and the vdW interaction direction a, the total energy changes smoothly with strain [apart from the bond breaking in Fig. 2(iii)] and no phase transition

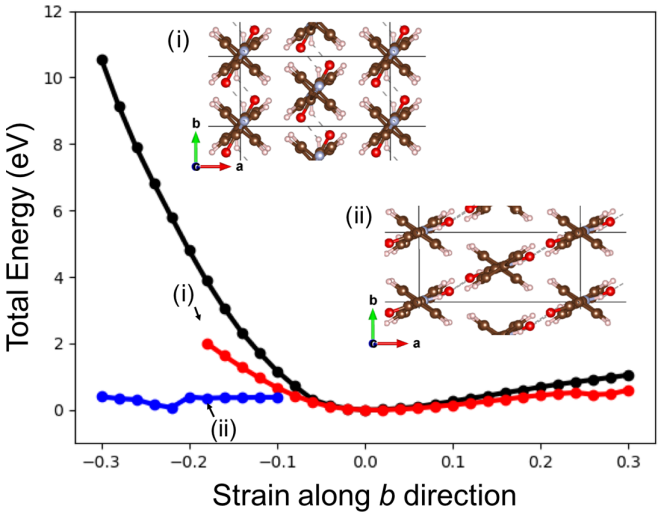

FIG. 3. Calculated total energies as a function of uniaxial strain along the *b* direction with the SCAN functional. The uniaxial strain case is shown by the curves in black, while the uniaxial stress case is illustrated by strain-energy curves in red for phase (i) and blue for phase (ii). The vertical axis is energy per two-molecule unit cell referred to that of the unstrained cell. The *ab* plane views of two PPTA phases under 18% compressive strain are shown in Figs. 3(i) and 3(ii).

is observed. The mechanical response is remarkably different along the hydrogen-bond interaction direction *b* as shown in Fig. 3. When no strain is applied, as shown in Fig. 1(i), the hydrogen bonds are all along the *b* direction through which a layered bonding network is formed in the *bc* plane. Upon large compressive strain along the *b* direction, those hydrogen bonds form a zigzag-shape connection [as shown in Fig. 3(ii)] along the *b* direction and oxygen atoms are pushed out of the original bonding planes towards the *a* direction. When these oxygen atoms are close enough to the hydrogen atoms in the neighboring layer, the original hydrogen-bond network breaks and is reorganized into a new layered hydrogen-bond structure along one diagonal of the *ab* rectangle. This change in the hydrogen-bond network clearly suggests a phase transition under compressive uniaxial stress along the *b* direction, at a critical strain of 10% and a critical stress of 25 Kbar. The two phases mentioned above correspond to the energy curves in red and blue, respectively, in Fig. 3. Interestingly, the total energy of the second phase (in blue) is not sensitive to the uniaxial stress along the *b* direction. This can be explained by the uniquely oriented hydrogen-bond network in this phase, as the sliding of the layers along the diagonal direction of the *ab* plane can effectively release the strain along the *b* direction without greatly changing the total energy.

The atomic coordination and lattice parameter information for the new phase (with 18% uniaxial compressive stress along the *b* direction) are included in the Supplemental Material [51]. The presence of imaginary modes in the calculated phonon spectrum for this new phase of PPTA suggests that the newly predicted phase may be associated with some structural instability, i.e., that the transition may occur to a structure other than the one we found. We also found that the new phase has an energy-minimizing volume at zero pressure, again with imaginary phonon frequencies.

Here we have used the SCAN density functional to predict a structural phase transition in PPTA. In many simpler materials [65,66], SCAN seems to be the best semilocal functional to describe such transitions. SCAN also accurately predicts the energies of the hydrogen-bond networks in various phases of ice [21] and in liquid water [55].

Young's modulus and yield strength are two very important physical quantities to determine the mechanical properties of PPTA under external mechanical deformation induced by an impact. Young's modulus can be defined as

$$Y = \frac{1}{V_0}\frac{\partial^2 E}{\partial \varepsilon^2}, \tag{1}$$

where E is the total energy, ε is the strain, and V_0 is the equilibrium volume of the system. Yield strength is the maximum stress that can be developed in a material without causing plastic deformation. From the calculated strain-energy correlation, we compute the Young's modulus and yield strength. As shown in Table II, we compare the Young's modulus and yield strength among four different functionals: PBE, PBE+rVV10L, SCAN, and SCAN+rVV10. Along the *c* direction, the Young's moduli calculated using all four functionals are close to each other. This is consistent with the similar curvatures of the strain-energy curves near the equilibrium positions as indicated in Fig. 2. The computed yield strengths are ranked as PBE < PBE+rVV10L ≈ SCAN+rVV10 ≈ SCAN. The yield is associated with the position of the last elastic deformation in Fig. 2(iii). The yield strength along the *c* direction is very high, which reveals the anisotropic mechanical

TABLE II. Young's modulus and yield strength (in GPa) of PPTA computed with different functionals. Experimental data for Kevlar® 29 and Kevlar® 49 [67] are shown in the table.

	c (chain)		*a* (vdW)		*b* (hydrogen bond)	
(GPa)	Young's modulus	Yield strength	Young's modulus	Yield strength	Young's modulus	Yield strength
Kevlar 29[a]	83	3.6				
Kevlar 49[a]	124	3.6				
PBE	296	28.6				
PBE+rVV10L	288	36.1	9	0.7	21	1.2
SCAN	299	38.1	9	0.5	30	1.4
SCAN+rVV10	316	35.9	15	1.5	31	1.9

[a]Reference [67].

performance of the PPTA crystal that needs special treatment for fiber synthesis.

We compare the calculated PPTA modulus and yield strength with the experimental data for Kevlar®29 and Kevlar®49 [67]. As shown in Table II, the experimental data are much smaller than the computed values (with a factor of 2 for Young's modulus and 10 for yield strength). This discrepancy is largely due to the fact that these Kevlar®29 and Kevlar®49 samples are fibers with a large number of PPTA molecular chains which are mechanically much weaker than perfect crystals. The computed Young's modulus is comparable with the previous computational result (252 GPa) obtained using B3LYP-D and PBE0-D functionals [17].

IV. CONCLUSION

PPTA is an ideal model system that contains three different types of interactions in a molecular crystal: covalent bonds, hydrogen bonds, and vdW interactions. We studied the structural and mechanical properties of PPTA by calculating equilibrium lattice parameters and applying strain along three lattice directions using first-principles calculations based on density functional theory with the SCAN, SCAN+rVV10, PBE+rVV10L, LDA, and PBE functionals. We found that the nonempirical SCAN functional (not fitted to any multicenter bonded system) indeed captures a large amount of medium-range vdW interaction and agrees very well with experiment for the lattice constants of the PPTA crystal. The SCAN+rVV10 functional overbinds the system due to the "double counting" of intermediate-range vdW interaction. The PBE functional does not capture enough vdW interaction and exhibits an incorrect bonding energy curve along the van der Waals axis. The pulling strength of the crystal along the chain direction is considerably larger than along the other two directions. When a large compressive stain is applied along the *b* (hydrogen bond) direction, a structural phase transition occurs. This transition, at an achievable 25 Kbar of uniaxial stress, is accompanied by a rotation of the hydrogen-bond network along the diagonal direction of the *ab* plane. We have computed Young's modulus and yield strength of PPTA and observe that the experimental data are much smaller than computationally predicted values for the PPTA crystal. This difference is attributed to the fact that these samples consisting of fibers are mechanically weaker than perfect molecular crystals.

While a long-range vdW correction to SCAN may not be needed for equilibrium geometries, it is still very much needed for the exfoliation energies of layered materials [28]. rVV10 is not the only choice for the long-range correction, and the damped Zaremba-Kohn (dZK) [64] correction is at least sometimes better.

ACKNOWLEDGMENTS

This work was supported by the Army Research Laboratory through Contract No. W911NF-16-2-0189 to Temple University. The work of H.P., who contributed to the calculations and the writing, was supported by the Center for Complex Materials from First Principles, an Energy Frontier Research Center funded by the US Department of Energy (DOE), Office of Science, Basic Energy Sciences (BES), under Award No. DE-SC0012575. This research includes calculations carried out on Temple University's HPC resources and thus was supported in part by the National Science Foundation through major research instrumentation Grant No. 1625061 and by the US Army Research Laboratory under Contract No. W911NF-16-2-0189. We thank S. Percec for comments on the manuscript.

[1] M. Lewin and J. Preston, *Handbook of Fiber Science and Technology/Vol. 3*, *High Technology Fibers, Pt. B*, edited by M. Lewin and J. Preston, International Fiber Science and Technology Series: Vol. 9 (Dekker, New York, 1989).

[2] H. Blades, High modulus, high tenacity poly(p-phenylene terephthalamide) fiber, U.S. Patent, US3869430A, 1975.

[3] H. G. Chae and S. Kumar, J. Appl. Polym. Sci. **100**, 791 (2006).

[4] R. J. Young, D. Lu, R. J. Day, W. F. Knoff, and H. A. Davis, J. Mater. Sci. **27**, 5431 (1992).

[5] M. G. Northolt and J. J. van Aartsen, J. Polym. Sci.: Polym. Lett. Ed. **11**, 333 (1973).

[6] M. Cheng, W. Chen, and T. Weerasooriya, J. Eng. Mater. Technol. **127**, 197 (2005).

[7] K. Tashiro, M. Kobayashi, and H. Tadokoro, Macromolecules **10**, 413 (1977).

[8] M. G. Northolt, Eur. Polym. J. **10**, 799 (1974).

[9] M. G. Dobb, D. J. Johnson, and B. P. Saville, J. Polym. Sci.: Polym. Phys. Ed. **15**, 2201 (1977).

[10] S. B. Warner, Macromolecules **16**, 1546 (1983).

[11] L. L. Chapoy, D. Spaseska, K. Rasmussen, and D. B. DuPré, Macromolecules **12**, 680 (1979).

[12] G. Washer, T. Brooks, and R. Saulsberry, J. Mater. Civ. Eng. **21**, 226 (2009).

[13] Y. Rao, A. J. Waddon, and R. J. Farris, Polymer **42**, 5937 (2001).

[14] S. F. Y. Li, A. J. McGhie, and S. L. Tang, Polymer **34**, 4573 (1993).

[15] J. O. Brauckmann, P. Zolfaghari, R. Verhoef, E. A. Klop, G. A. de Wijs, and A. P. M. Kentgens, Macromolecules **49**, 5548 (2016).

[16] G. C. Rutledge, U. W. Suter, and C. D. Papaspyrides, Macromolecules **24**, 1934 (1991).

[17] L. Avanzini, L. Brambilla, C. Marano, and A. Milani, Polymer **116**, 133 (2017).

[18] L. Kronik and A. Tkatchenko, Acc. Chem. Res. **47**, 3208 (2014).

[19] E. F. C. Byrd, G. E. Scuseria, and C. F. Chabalowski, J. Phys. Chem. B **108**, 13100 (2004).

[20] J. W. Sun, A. Ruzsinszky, and J. P. Perdew, Phys. Rev. Lett. **115**, 036402 (2015).

[21] J. Sun *et al.*, Nat. Chem. **8**, 831 (2016).

[22] D. M. Ceperley and B. J. Alder, Phys. Rev. Lett. **45**, 566 (1980).

[23] H. Peng and J. P. Perdew, Phys. Rev. B **95**, 081105(R) (2017).

[24] M. Shahbaz and K. Szalewicz, Phys. Rev. Lett. **121**, 113402 (2018).

[25] M. J. DelloStritto, S. M. Piontek, M. L. Klein, and E. Borguet, J. Phys. Chem. Lett. **10**, 2031 (2019).

[26] R. Sabatini, T. Gorni, and S. de Gironcoli, Phys. Rev. B **87**, 041108(R) (2013).

[27] O. A. Vydrov and T. V. Voorhis, J. Chem. Phys. **133**, 244103 (2010).

[28] H. W. Peng, Z. H. Yang, J. P. Perdew, and J. W. Sun, Phys. Rev. X **6**, 041005 (2016).

[29] H. Rydberg, M. Dion, N. Jacobson, E. Schröder, P. Hyldgaard, S. I. Simak, D. C. Langreth, and B. I. Lundqvist, Phys. Rev. Lett. **91**, 126402 (2003).

[30] K. Berland and P. Hyldgaard, Phys. Rev. B **89**, 035412 (2014).

[31] A. D. Becke and E. R. Johnson, J. Chem. Phys. **122**, 154104 (2005).

[32] H. Tang, J. Tao, A. Ruzsinszky, and J. P. Perdew, J. Phys. Chem. C **123**, 13748 (2019).

[33] J. Klimeš and A. Michaelides, J. Chem. Phys. **137**, 120901 (2012).

[34] K. E. Riley, M. Pitoňák, P. Jurečka, and P. Hobza, Chem. Rev. **110**, 5023 (2010).

[35] A. Tkatchenko, L. Romaner, O. T. Hofmann, E. Zojer, C. Ambrosch-Draxl, and M. Scheffler, MRS Bull. **35**, 435 (2010).

[36] L. Goerigk, J. Chem. Theory Comput. **10**, 968 (2014).

[37] R. Balu, E. F. C. Byrd, and B. M. Rice, J. Phys. Chem. B **115**, 803 (2011).

[38] S. Grimme, Wiley Interdiscip. Rev.: Comput. Mol. Sci. **1**, 211 (2011).

[39] L. Goerigk and S. Grimme, J. Chem. Theory Comput. **7**, 291 (2011).

[40] T. Risthaus and S. Grimme, J. Chem. Theory Comput. **9**, 1580 (2013).

[41] J. Moellmann and S. Grimme, J. Phys. Chem. C **118**, 7615 (2014).

[42] J. Moellmann and S. Grimme, Phys. Chem. Chem. Phys. **12**, 8500 (2010).

[43] L. Maschio, B. Civalleri, P. Ugliengo, and A. Gavezzotti, J. Phys. Chem. A **115**, 11179 (2011).

[44] J. G. Brandenburg and S. Grimme, J. Phys. Chem. Lett. **5**, 1785 (2014).

[45] A. M. Reilly and A. Tkatchenko, J. Phys. Chem. Lett. **4**, 1028 (2013).

[46] A. M. Reilly and A. Tkatchenko, J. Chem. Phys. **139**, 024705 (2013).

[47] N. Marom, R. A. DiStasio, Jr., V. Atalla, S. Levchenko, A. M. Reilly, J. R. Chelikowsky, L. Leiserowitz, and A. Tkatchenko, Angew. Chem. Int. Ed. **52**, 6629 (2013).

[48] A. M. Reilly and A. Tkatchenko, Chem. Sci. **6**, 3289 (2015).

[49] A. M. Reilly and A. Tkatchenko, Phys. Rev. Lett. **113**, 055701 (2014).

[50] A. Zen, J. G. Brandenburg, J. Klimeš, A. Tkatchenko, D. Alfè, and A. Michaelides, Proc. Natl. Acad. Sci. USA **115**, 1724 (2018).

[51] See Supplemental Material at http://link.aps.org/supplemental/10.1103/PhysRevMaterials.4.055601 for a brief discussion on some recent long-range vdW corrections and the structural information of the new phase of strained PPTA.

[52] J. P. Perdew, K. Burke, and M. Ernzerhof, Phys. Rev. Lett. **77**, 3865 (1996).

[53] G. Kresse and J. Furthmuller, Comput. Mater. Sci. **6**, 15 (1996).

[54] P. E. Blöchl, Phys. Rev. B **50**, 17953 (1994).

[55] M. Chen *et al.*, Proc. Natl. Acad. Sci USA **114**, 10846 (2017).

[56] J. Wiktor, F. Ambrosio, and A. Pasquarello, J. Chem. Phys. **147**, 216101 (2017).

[57] J. G. Brandenburg, J. E. Bates, J. Sun, and J. P. Perdew, Phys. Rev. B **94**, 115144 (2016).

[58] J. Hermann and A. Tkatchenko, J. Chem. Theory Comput. **14**, 1361 (2018).

[59] E. B. Isaacs and C. Wolverton, Phys. Rev. Materials **2**, 063801 (2018).

[60] Y. Fu and D. J. Singh, Phys. Rev. Lett. **121**, 207201 (2018).

[61] J. W. Furness, J. P. Perdew, and J. Sun (unpublished).

[62] S. Adhikari, H. Tang, B. Neupane, A. Ruzsinszky, and G. I. Csonka, Phys. Rev. Materials **4**, 025005 (2020).

[63] J. Tao, H. Tang, A. Patra, P. Bhattarai, and J. P. Perdew, Phys. Rev. B **97**, 165403 (2018).

[64] H. Tang, S. T. U. R. Chowdhury, J. Tao, and J. P. Perdew (unpublished).

[65] C. Shahi, J. Sun, and J. P. Perdew, Phys. Rev. B **97**, 094111 (2018).

[66] N. Sengupta, J. E. Bates, and A. Ruzsinszky, Phys. Rev. B **97**, 235136 (2018).

[67] H. H. Yang, *Kevlar Aramid Fiber: Technical Guide* (Dupont, New York, 1992).